Green Mechanochemical Synthesis of Binary and Ternary Cadmium Chalcogenides with Tunable Band Gaps

Matjaž Kristl * , Neža Zanjkovič , Jona Kunej , Sašo Gyergyek , Janja Stergar

Posted Date: 3 October 2025

doi: 10.20944/preprints202510.0291.v1

Keywords: cadmium; sulfide; selenide; telluride; ternary compounds; mechanochemistry; band gap

Article

Green Mechanochemical Synthesis of Binary and Ternary Cadmium Chalcogenides with Tunable Band Gaps

Matjaž Kristl [1,*], Neža Zanjkovič [1], Jona Kunej [1], Sašo Gyergyek [1,2] and Janja Stergar [1]

[1] Faculty of Chemistry and Chemical Engineering, University of Maribor, Smetanova 17, SI-2000 Maribor, Slovenia

[2] Jožef Stefan Institute, Department of Materials Synthesis, Jamova 39, SI-1000 Ljubljana, Slovenia

* Correspondence: matjaz.kristl@um.si

Abstract

In this work, we report on the mechanochemical preparation and characterization of binary (CdS, CdSe, and CdTe) and ternary ($CdS_{0.5}Se_{0.5}$, $CdS_{0.5}Te_{0.5}$, and $CdSe_{0.5}Te_{0.5}$) cadmium chalcogenides. The compounds were synthesized in a planetary micro mill using a zirconia grinding bowl and zirconia grinding balls. The products were examined by powder X-ray diffraction (pXRD), transmission electron microscopy (TEM), energy-dispersive X-ray spectroscopy (EDX), dynamic light scattering (DLS), UV-Vis spectroscopy, and differential scanning calorimetry (DSC). The materials were obtained in the form of irregularly shaped aggregates measuring up to several hundred nanometers, composed of nearly spherical primary nanoparticles with diameters in the 10–20 nm range. The band gap energies calculated using *Tauc* plots for $CdS_{0.5}Se_{0.5}$, $CdS_{0.5}Te_{0.5}$, and $CdSe_{0.5}Te_{0.5}$, were 2.01 eV, 1.72 eV, and 1.53 eV, respectively. These results demonstrate the expected tunability of band gaps in ternary cadmium chalcogenides and attest to the potential of such materials for semiconducting applications, particularly in solar cells. The mechanochemical approach is once again shown to be a simple and effective method for the preparation of both binary and ternary chalcogenides, avoiding the use of solvents, toxic precursors, and energy-consuming reaction conditions.

Keywords: cadmium; sulfide; selenide; telluride; ternary compounds; mechanochemistry; band gap

1. Introduction

Cadmium chalcogenides, namely cadmium sulfide (CdS), cadmium selenide (CdSe), and cadmium telluride (CdTe), represent an important class of II–VI semiconductor materials with wide-ranging applications in optoelectronics, photovoltaics, and luminescent devices. Cadmium sulfide with a direct band gap of 2.42 eV was reported to possess immense potential applications in LED diodes and solar cells already two decades ago [1] and has recently been under intense investigation due to its outstanding catalytic, optical, and electronic properties, enabling its use in photocatalytic water splitting [2–4]. Cadmium selenide has served as the subject of many studies due to its good application prospects in optoelectronic devices [5]. The insertion of alkali metals and group 12 metals has led to the synthesis of a large group of chalcogenides with desirable electrical and optical properties [6,7].

Beyond these binary compounds, their ternary and quaternary solid solutions allow fine-tuning of band gaps and optical properties, thereby expanding their technological potential [8]. In particular, Cd-based ternary and quaternary (CdSeTe and CdSSeTe) compounds have shown superior properties that can be controlled by managing the composition, even without changing the particles' size [9]. As an instance, the CdS : CdSe ternary system has been reported to exhibit a perfect choice for photodetectors due to its wide adjustable band gap range [10]. CdSSe/ZnS nanocomposites were

 doi:10.20944/preprints202510.0291.v1

reported for their applications in quantum-dot light-emission diodes (qLED) [11] while CdSeS 'magic-size' clusters have shown potential for applications for light scavenging and bioimaging [12].

Among the cadmium chalcogenides, cadmium telluride CdTe holds a prominent position as a II–VI semiconductor that has been widely investigated for its favorable optoelectronic properties [13]. With a direct band gap of ~1.5 eV, close to the Shockley–Queisser optimum for single-junction solar cells, and a high absorption coefficient, CdTe efficiently absorbs sunlight even in very thin layers [14,15]. These properties make it particularly attractive for thin-film photovoltaics, where CdTe-based devices have achieved competitive conversion efficiencies while maintaining lower production costs compared to crystalline silicon [16]. Today, CdTe solar cells represent one of the most commercially mature thin-film technologies and continue to play a key role in the development of scalable, high-efficiency, and cost-effective renewable energy systems [16–18].

While conventional methods for the synthesis of transition metal chalcogenides have long been known and established, they have key shortcomings that make them incompatible with the principles of green chemistry: they often require high temperatures, toxic precursors, or complex processing steps [19–21]. Among alternative preparation methods, which have been gaining popularity over the last decades, the single-source precursor method has emerged as an attractive approach for synthesizing metal chalcogenides, as both the metal and chalcogen are incorporated within one molecule, enabling better stoichiometric control [20–22]. While this method was also successfully applied during our previous research [23], it has a serious impediment due to the limited number of potential ligands containing sulfur, selenium and especially tellurium. Another method, which has emerged over the past two decades as a valuable technique for synthesizing nanostructured materials, is the sonochemical process. Ultrasound causes the phenomenon called *acoustic cavitation*, i.e., the formation, growth, and implosive collapse of gas bubbles in the sonicated solution or slurry. This process causes transitory high temperatures and pressures as well as rapid cooling rates, which can be exploited to create nanoparticles [20]. The sonochemical method was successfully applied during our previous research for the synthesis of binary CdS, CdSe, and CdTe nanoparticles in aqueous solutions [24,25] and was also successfully utilized for producing hexagonal CdS nanoplatelets in a continuous reactor [26]. Nevertheless, the aforementioned method obviously encounters its limitations when it comes to the synthesis of ternary compounds [27].

In contrast, the mechanochemical synthesis has emerged as a simple, energy-efficient, and environmentally benign alternative, enabling direct solid-state reactions at room temperature, in most cases without the need for solvents [19]. Mechanochemical reactions are the result of chemical transformations, occurring from grinding, milling, and alloying solid precursors. The method is carried out at relatively low temperatures (i.e., without external energy input), is reported to be reproducible, simple, and easy to operate, ensuring a high yield and control of the particle size by changing the milling conditions [20,28,29]. This approach offers advantages such as reduced reaction times, scalability, and the possibility of accessing metastable phases, making it an attractive and 'green' method for producing cadmium chalcogenides and their alloys [30,31]. While traditionally limited to niche applications, mechanochemistry has recently evolved from a laboratory curiosity to a powerful tool for the synthesis of nanosized materials [32], especially when combined with other energy sources like light irradiation, sound agitation, or electrical impulses [33]. Among other possible applications, the mechanochemical synthesis of nanoparticles for potential antimicrobial applications was reported recently [34].

Although mechanochemical syntheses of binary transition metal chalcogenides have been reported extensively in the literature, the first one being published more than two decades ago [35], this topic remains an active area of research. While the mechanochemical method is clearly suitable for the synthesis of binary chalcogenides [36,37], including the preparation of Cu, Cd, Al, Ga, and Ni chalcogenides reported in previous papers published by our group [38–40], the extension of this approach to ternary cadmium chalcogenides has, to the best of our knowledge, not yet been described and therefore represents the novel contribution of the present study.

 doi:10.20944/preprints202510.0291.v1

2. Materials and Methods

2.1. Ball Milling

All reagents used were commercially available and employed without additional purification. Cadmium (powder, ~100 mesh, 99.5% trace metal basis) and tellurium (powder, 200 mesh, 99.8% trace metal basis) were obtained from Sigma-Aldrich, St. Louis, MO, USA. Selenium powder was acquired from Kemika d.d., Zagreb, Croatia, while sulfur (powder, 99.98%) was obtained from Merck KGaA, Darmstadt, Germany. The treatment of the mixtures was performed in a Fritsch premium line PULVERISETTE 7 Planetary Micro Mill (Fritsch, Idar-Oberstein, Germany) equipped with a 20 mL zirconia griding bowl and 10 mm diameter zirconia grinding balls. During all experiments, we used 10 milling balls (with a total mass of ≈ 30 g) and a 15 : 1 ball-to-powder mass ratio. As an example: for the synthesis of $CdS_{0.5}Se_{0.5}$, we weighed 1.3388 g (= 11.91 mmol) of Cd, 0.1909 g (= 5.95 mmol) of S, and 0.4703 g (= 5.96 mmol) of Se, to satisfy both the conditions: $n(S) + n(Se) = n(Cd)$ and $m(S) + m(Se) + m(Cd) \approx 2$ g. The masses of precursors during other experiments were calculated based on the same assumptions. To prevent overheating, the milling was conducted in 15 min intervals, followed by 15 min breaks. While initial experiments were performed in air atmosphere, we used argon atmosphere during some of the subsequent experiments to prevent oxidation, as explained further on.

2.2. Characterization

Powder X-ray diffraction (pXRD) data were collected on a PANalytical X'pert PRO diffractometer, (Malvern Panalytical Ltd., Malvern, UK) using CuKα1 radiation (λ = 1.5406 Å), scanning range from 10° to 70°, step size 0.02° and time/step = 1 s. Transmission electron microscopy (TEM) measurements were performed using a JEOL 2100 microscope (JEOL Inc., Peabody, MA, USA). The obtained powders were dispersed in isopropanol using an ultrasonic bath and placed on a carbon-coated copper grid. The elemental composition of the particles was analyzed using a Jeol JED 2300 EDXS system, (JEOL Inc., Peabody, MA, USA). The hydrodynamic particle size was measured by dynamic light scattering (DLS) with Zetasizer Nano-S equipment (Malvern Instruments, Malvern, UK) using disposable 1 cm polystyrene cuvettes. A UV-VIS spectrometer Varian Cary 50 Bio (Varian Inc., Palo Alto, CA, USA) was used to study the optical properties of the prepared cadmium chalcogenides. The samples were dispersed in ethanol in an ultrasonic bath prior to the measurement. The cadmium content was measured on a Varian SpectrAA-10 flame atomic spectrometer (AAS) (Varian Inc., Palo Alto, CA, USA) after digestion of the samples [41] with concentrated HNO_3 in PTFE vessels in a microwave oven (MDS-2000, CEM Corporation, Matthews, NC, USA). Thermal analysis of the samples was carried out by Mettler DSC 3 (Mettler Toledo, Switzerland) in 40 μL aluminum crucibles, using a heating rate of 10 K/min and a temperature range from 30 to 600 °C.

3. Results and Disussion

3.1. Binary Mixtures

Powder X-ray diffraction (pXRD) patterns of products obtained by ball milling equimolar Cd:S, Cd:Se, and Cd:Te mixtures for 15 min are shown in Figures 1–3. In the case of the Cd : S system (Figure 1), all major reflections correspond to hexagonal CdS (ICDD PDF-4, file No. 00-006-0314). When milling was carried out in air, additional peaks attributable to CdO (ICDD file No. 00-005-0640) were observed. This oxidation was effectively suppressed when the milling was performed under an argon atmosphere, yielding phase-pure CdS. The Cd:Se system exhibited analogous behavior (Figure 2). The main product was cubic CdSe (ICDD file No. 00-019-0191), while minor CdO reflections appeared in samples prepared in air. As in the case of CdS, performing the reaction under argon completely prevented CdO formation. In contrast, the mechanochemical reaction of Cd and Te

 doi:10.20944/preprints202510.0291.v1

consistently yielded single-phase cubic CdTe (ICDD file No. 00-015-0770), even when milling was conducted in air (Figure 3), with no CdO impurities detected.

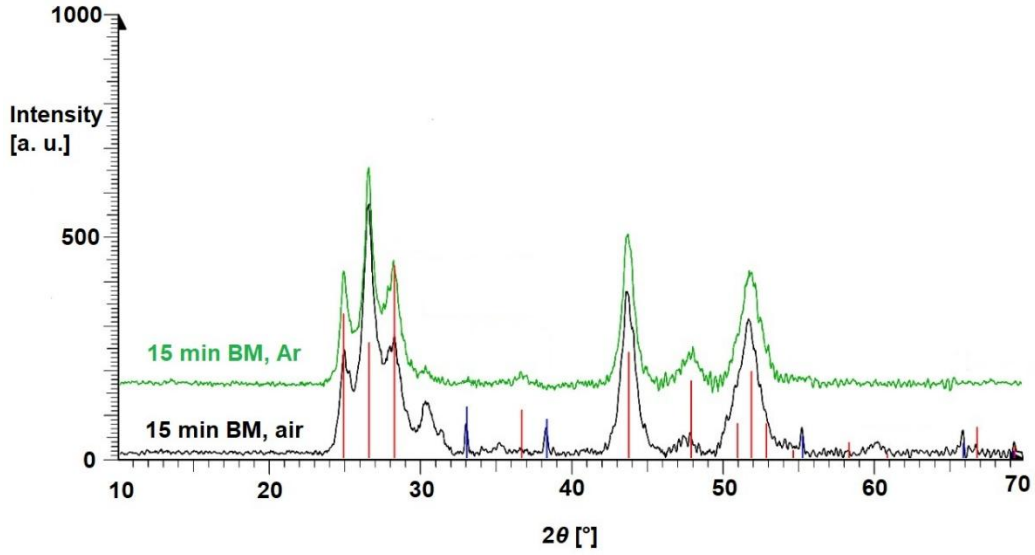

Figure 1. XRD patterns of CdS, prepared mechanochemically after 15 min milling time. Red and blue vertical bars represent CdS and CdO, respectively.

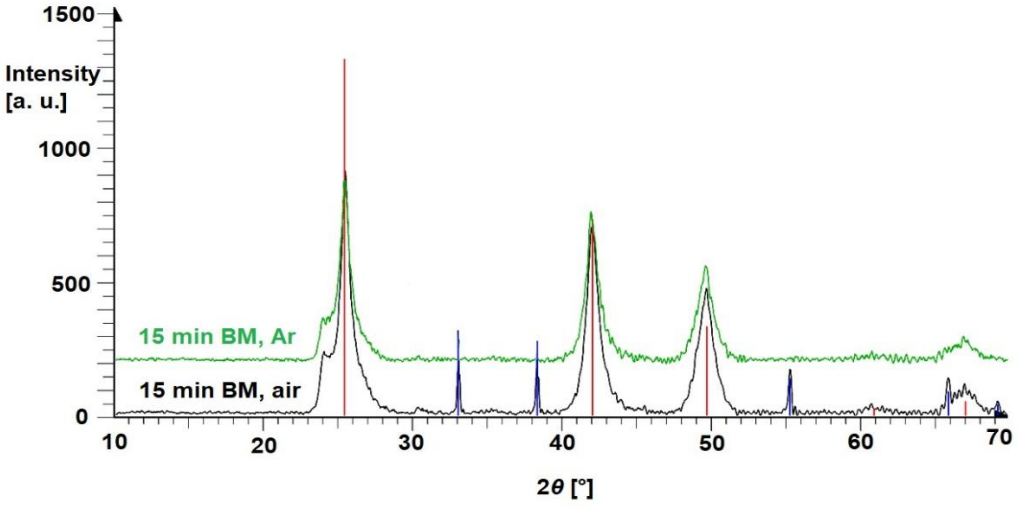

Figure 2. XRD patterns of CdSe, prepared mechanochemically after 15 min milling time. Red and blue vertical bars represent CdSe and CdO, respectively.

 doi:10.20944/preprints202510.0291.v1

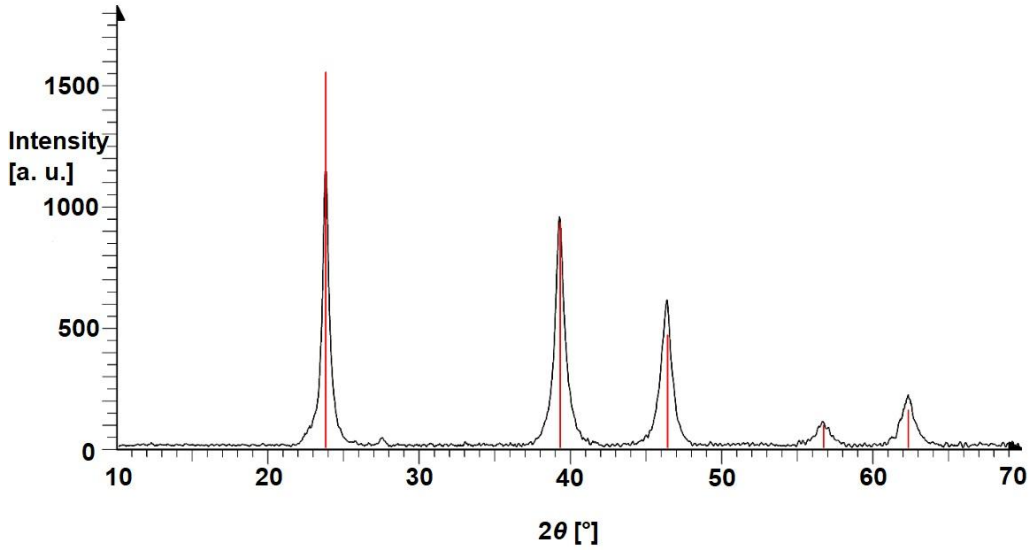

Figure 3. XRD patterns of CdTe, prepared mechanochemically after 15 min milling time. Red vertical bars represent CdTe, as reported in the ICDD database.

The pXRD results were further confirmed by DSC measurements for all precursors and ball-milled products, as presented in Figures 4 (a) – (c). For the Cd:S system (Figure 4a), the DSC curves of both elemental precursors display pronounced endothermic peaks corresponding to the melting points of Cd (T_m = 321 °C) and S (T_m = 119 °C). The minor endothermic peaks on the DSC curve of sulfur correspond to Sα → Sβ and Sβ → Sγ transitions [42] and the endotherm occurring at T ≈ 400 °C indicates the boiling point of sulfur; however, the changes beyond the melting point can be considered to be irrelevant to the discussion. After 15 min of milling, none of the precursor melting peaks remain, indicating complete conversion into CdS. This is consistent with the high melting point of CdS (≈ 1750 °C), which lies well beyond the accessible range of conventional DSC. The DSC curve of the product obtained after 60 min of milling is indistinguishable from that after 15 min, further confirming the rapid and complete formation of CdS. For comparison, a sample prepared by simple mortar-and-pestle grinding for ~ 5 min was also analyzed. Its DSC curve still shows both precursor melting peaks, albeit with significantly reduced intensity, suggesting that the reaction is initiated even under such mild mechanical treatment. A similar phenomenon was previously reported for the mechanochemical synthesis of CuS [38].

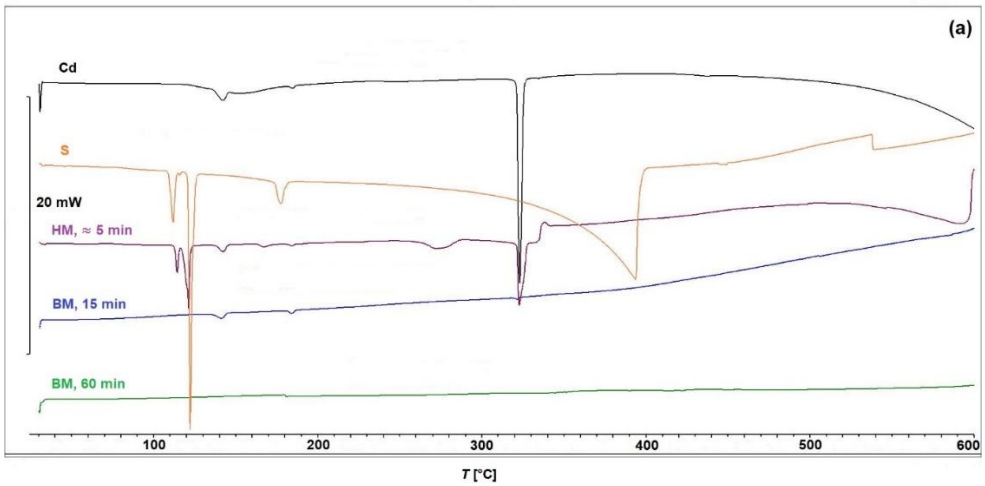

 doi:10.20944/preprints202510.0291.v1

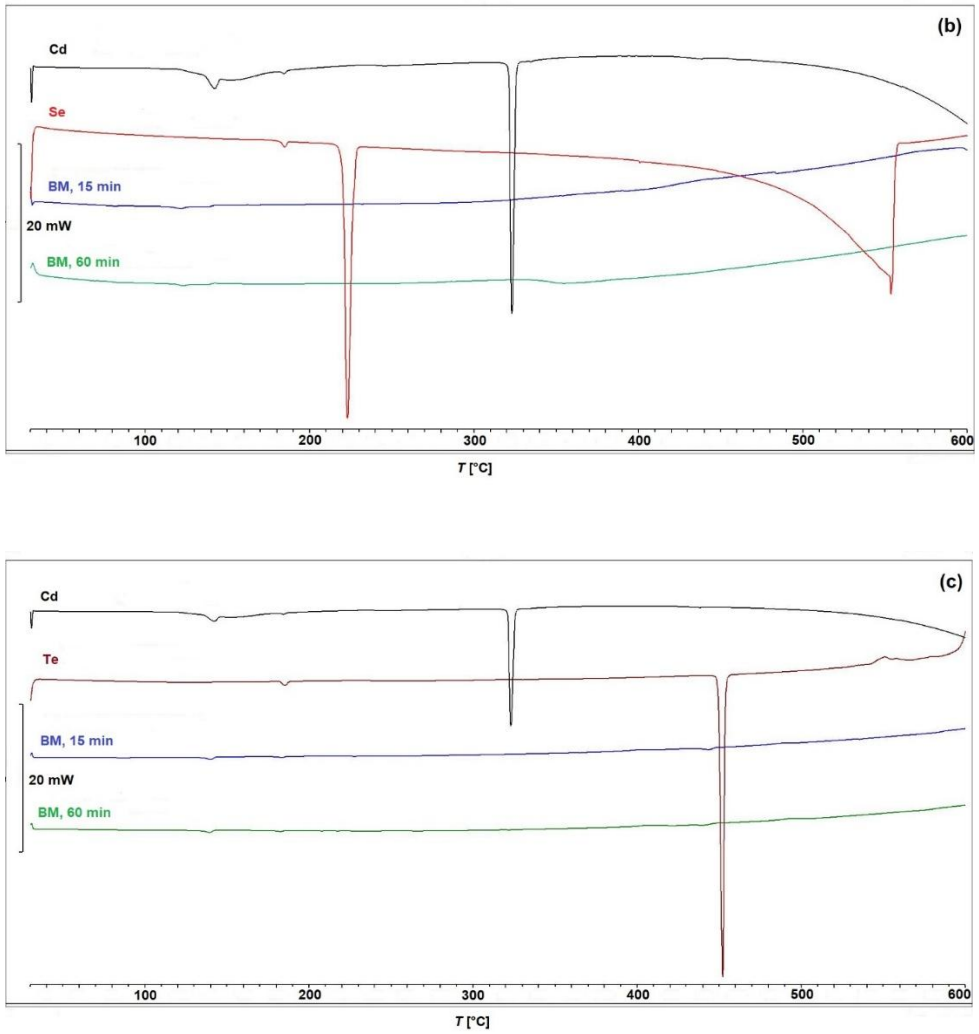

Figure 4. DSC curves of corresponding elemental precursors and binary chalcogenides, obtained by 15 min and 60 min ball milling for the Cd : S system (a), Cd : Se system (b), and Cd : Te system (c).

For the Cd:Se system (Figure 4b), the DSC curve of elemental selenium shows a sharp endothermic peak at ~221 °C, corresponding to its melting point. After 15 min of milling, the melting peaks of both precursors are absent, indicating complete conversion to CdSe. Extending the milling time to 60 min produces no further changes, confirming the rapidity of the reaction. Analogous behavior was observed for the Cd:Te system (Figure 4c). The DSC curve of tellurium exhibits a sharp endothermic peak at ~449 °C, corresponding to its melting point. After 15 min of milling, this peak disappears, consistent with complete reaction to CdTe. As CdTe has a melting point close to 1100 °C [43], no product-related endotherms can be detected within the accessible DSC temperature range.

The binary systems thus demonstrate that mechanochemical synthesis enables the rapid and complete formation of CdS, CdSe, and CdTe within 15 min of milling, with phase purity dependent only on the milling atmosphere in the cases of CdS and CdSe. Having established the efficiency and reliability of the method for binary cadmium chalcogenides, attention was next directed to ternary Cd–S–Se–Te systems. These compounds are of particular interest because their tunable compositions enable adjustment of structural and electronic properties, making them attractive for optoelectronic and photovoltaic applications.

3.2. Ternary Mixtures

Powder diffraction patterns of CdS_xSe_{1-x} samples, prepared using two different S : Se ratios, are presented in Figures 5 (a) and 5 (b). The pattern of the sample, prepared by using a S : Se = 0.5 : 0.5

 doi:10.20944/preprints202510.0291.v1

ratio, is shown together with those of both binary compounds, i.e., CdS and CdSe, in Figure 5 (a). Although no ICDD reference exists for $CdS_{0.5}Se_{0.5}$, the observed reflections fall almost exactly midway between the signals of CdS and CdSe, consistent with the formation of a solid solution. The sample prepared by using a S : Se = 0.8 : 0.2 ratio (Figure 5 (b)), matches perfectly with the pattern of ICDD file No. 00-040-0837, reported therein as '$Cd_{10}S_{8.13}Se_{1.87}$'. Notably, in contrast to the binary CdS and CdSe systems, no peaks of CdO were detected, even when milling was conducted in air.

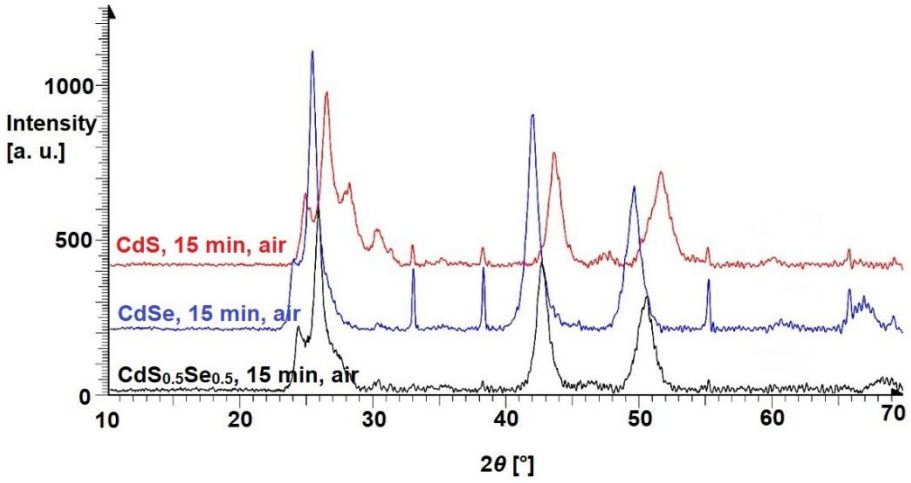

(**a**)

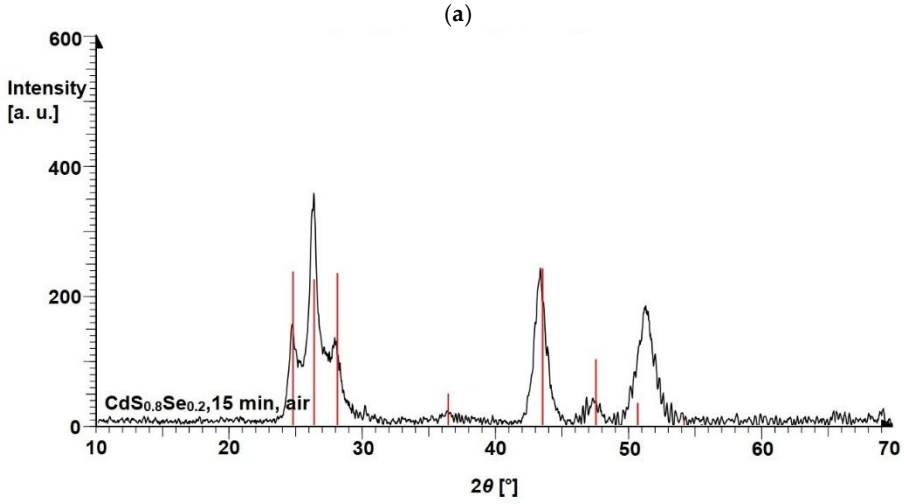

(**b**)

Figure 5. (a). XRD patterns of ternary $CdS_{0.5}Se_{0.5}$, prepared mechanochemically after 15 min milling time. The patterns of the binary compounds, CdS and CdSe, are shown for comparison. **(b).** XRD patterns of ternary $CdS_{0.8}Se_{0.2}$, prepared mechanochemically after 15 min milling time. The red vertical bars represent '$Cd_{10}S_{8.13}Se_{1.87}$', as reported in the ICDD database.

A comparable outcome was obtained for the CdS_xTe_{1-x} system. The diffraction pattern of the sample with S:Te = 0.5:0.5 (Figure 6) displays reflections located midway between those of CdS and CdTe. No ICDD reference exists for $CdS_{0.5}Te_{0.5}$, however the absence of CdO peaks indicate that, as with CdS_xSe_{1-x}, no CdO could be detected even when milling was performed in air.

 doi:10.20944/preprints202510.0291.v1

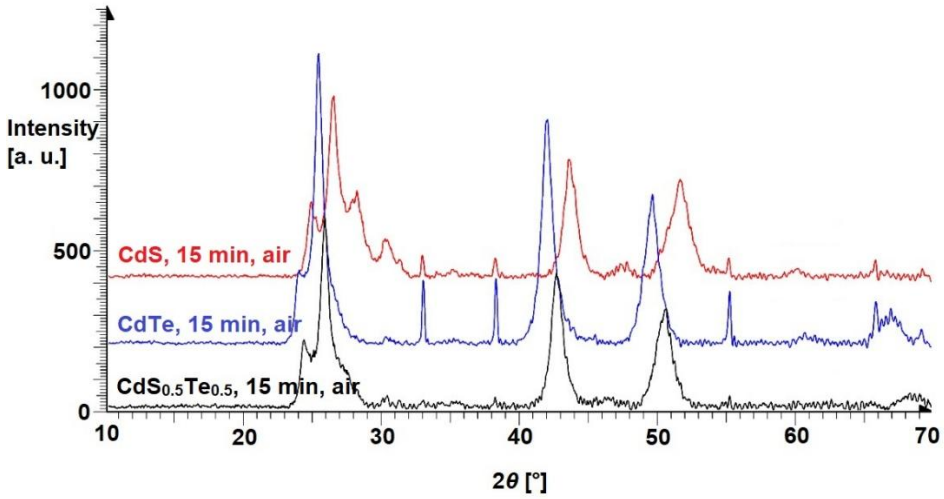

Figure 6. XRD patterns of ternary $CdS_{0.5}Te_{0.5}$, prepared mechanochemically after 15 min milling time. The patterns of the binary compounds, CdS and CdTe, are shown for comparison.

Finally, diffraction patterns for the $CdSe_xTe_{1-x}$ system are depicted in Figure 7. Analogous to the previous two examples, the peaks of $CdSe_{0.5}Te_{0.5}$ are located between those of both binary chalcogenides. Although no ICDD reference exists for $CdS_{0.5}Te_{0.5}$, the measured peaks correspond closely to the reported pattern of hexagonal $CdSe_{0.6}Te_{0.4}$, (ICDD file No. 00-041-1325).

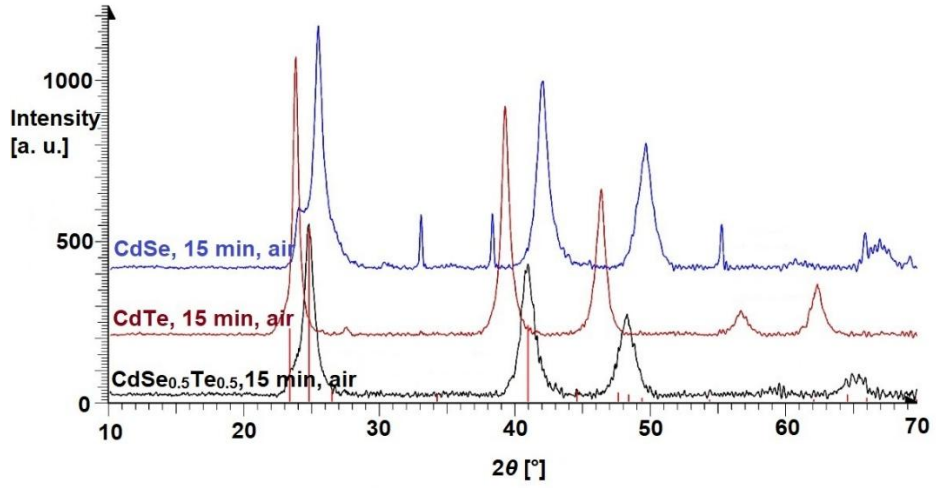

Figure 7. XRD patterns of ternary $CdSe_{0.5}Te_{0.5}$, prepared mechanochemically after 15 min milling time. The patterns of the binary compounds, CdSe and CdTe, are shown for comparison. The red vertical bars represent $CdSe_{0.6}Te_{0.4}$, as reported in the ICDD database.

As with the binary systems, the pXRD findings were complemented by DSC measurements performed on all precursors and products, as presented in Figures 8 (a) – (c). In all three ternary systems, no precursor melting peaks were observed after 15 min of milling, confirming complete conversion. Prolonged milling up to 60 min produced no significant changes in the DSC curves, indicating that the reactions are already completed within the initial 15 min.

 doi:10.20944/preprints202510.0291.v1

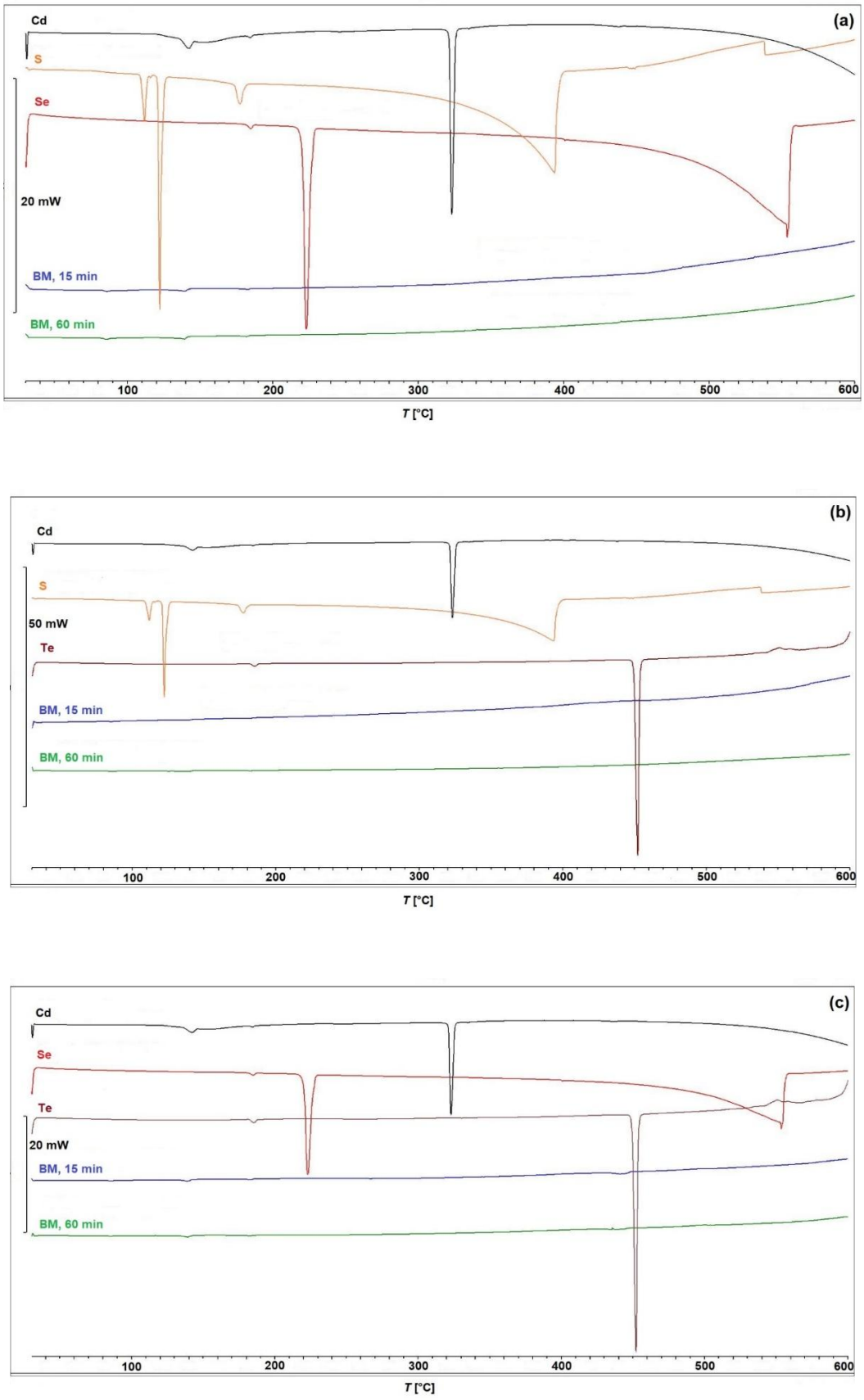

Figure 8. DSC curves of corresponding elemental precursors and ternary chalcogenides, obtained by 15 min and 60 min ball milling for the Cd : S : Se system (a), Cd : S : Te system (b), and Cd : Se : Te system (c).

The crystallite sizes of all products were calculated using the *Scherrer* equation:

 doi:10.20944/preprints202510.0291.v1

$$d_x = \frac{0{,}94 \cdot \lambda \cdot 57{,}3}{\beta \cdot \cos\theta}$$

Here, λ is the wavelength of the X – ray radiation (nm), β the full – width at half – maximum (FWHM) of the corresponding peak (°) and θ is the diffraction angle (°). The results, presented in Table 1, were obtained by calculating the average value of 2 – 3 most prominent peaks.

Table 1. Crystallite sizes of binary and ternary cadmium chalcogenides after 15 min milling time, calculated from the pXRD data using *Scherrer* equation.

sample	CdS	CdSe	CdTe	$CdS_{0.8}Se_{0.2}$	$CdS_{0.5}Se_{0.5}$	$CdS_{0.5}Te_{0.5}$	$CdSe_{0.5}Te_{0.5}$
d [nm]	11.1	11.2	16.9	13.7	11.6	10.4	10.3

The morphology of the binary products obtained after 15 min of milling was examined by TEM (Figures 9 (a) – (c)). All samples consist of irregularly shaped aggregates with dimensions extending up to several hundred nanometers, a feature commonly observed in mechanically milled products due to the intense forces exerted during the process [40]. Closer inspection suggests the presence of smaller, nearly spherical primary nanoparticles with diameters in the 10–20 nm range. These dimensions are broadly consistent with crystallite sizes estimated from pXRD data using the Scherrer equation, although the clustered nature of the samples limits a more precise assessment. Results of the EDX analysis correspond well to the results obtained by pXRD and to Cd content, determined by AAS: 77.4 wt.% Cd for CdS (calc. 77.8%), 58.5 wt.% Cd for CdSe (calc. 58.7%), 46.3 wt.% Cd for CdTe (calc. 46.8%).

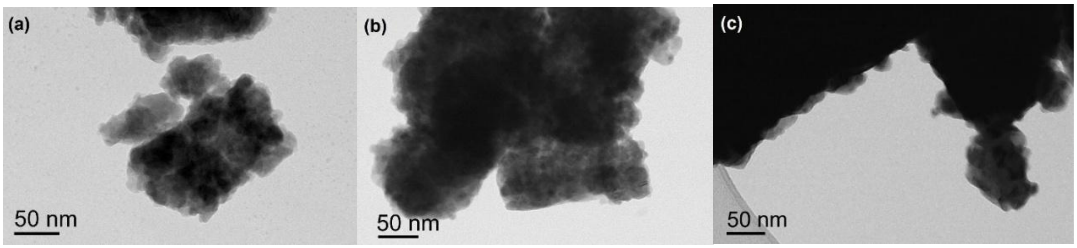

Figure 9. TEM images of binary chalcogenides CdS (a), CdSe (b), and CdTe (c) after 15 min milling times.

Similar conclusions can be drawn from TEM images of selected ternary products ($CdS_{0.5}Se_{0.5}$, $CdS_{0.5}Te_{0.5}$, and $CdSe_{0.5}Te_{0.5}$), as presented in Figures 10 (a) – 10 (c). At higher magnifications, the presence of spherical primary nanoparticles is more clearly visible, as depicted in Figures 11 (a) – 11 (c). AAS results for ternary products again showed good agreement with the data obtained from EDX and pXRD: 66.5 wt.% Cd for $CdS_{0.5}Se_{0.5}$ (calc. 66.9%), 58.5 wt.% Cd for $CdS_{0.5}Te_{0.5}$ (calc. 58.5%) and, 51.9 wt.% Cd for $CdSe_{0.5}Te_{0.5}$ (calc. 52.1%).

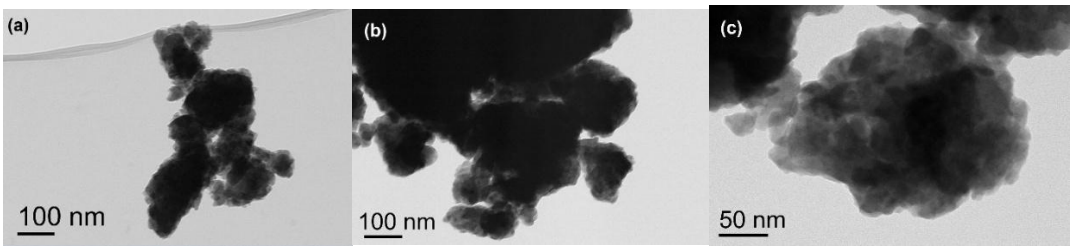

Figure 10. TEM images of ternary chalcogenides $CdS_{0.5}Se_{0.5}$ (a), $CdS_{0.5}Te_{0.5}$ (b), and $CdSe_{0.5}Te_{0.5}$ (c) after 15 min milling times.

 doi:10.20944/preprints202510.0291.v1

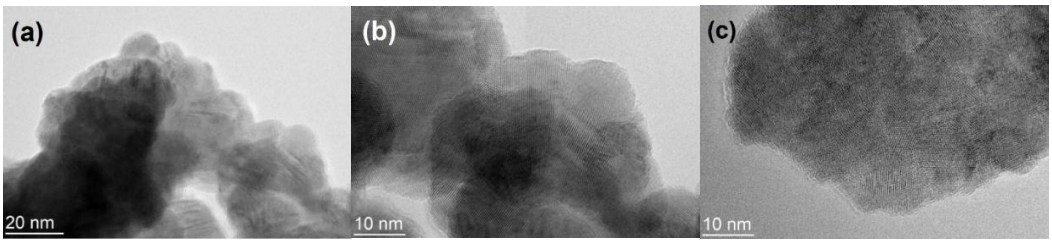

Figure 11. TEM images of ternary chalcogenides $CdS_{0.5}Se_{0.5}$ (a and b), and $CdSe_{0.5}Te_{0.5}$ (c) after 15 min milling times, showing primary spherical nanoparticles under higher magnifications.

Particle size measurements and hydrodynamic size distribution were additionally corroborated by DLS measurements in water suspensions after applying an ultrasonic bath. For each of the samples, three independent measurements were performed and the average value calculated. The results are presented in Table 2. As expected, the hydrodynamic diameters obtained by DLS are significantly larger than crystallite sizes estimated from pXRD or the primary nanoparticle dimensions suggested by TEM. This discrepancy is well known and arises because DLS measures the apparent size of particles as they diffuse in suspension, which includes contributions from solvation layers and possible particle agglomeration in liquid media [40,44,45]. Within this general trend, the CdTe and $CdSe_{0.5}Te_{0.5}$ samples appear to exhibit comparatively smaller hydrodynamic sizes, although the origin of this behavior is not yet clear and would require more systematic investigation.

Table 2. Hydrodynamic diameter of binary and ternary cadmium chalcogenides after 15 min milling time, obtained from DSL measurements.

sample	CdS	CdSe	CdTe	$CdS_{0.8}Se_{0.2}$	$CdS_{0.5}Se_{0.5}$	$CdS_{0.5}Te_{0.5}$	$CdSe_{0.5}Te_{0.5}$
d(H) [nm]	325.8	202.7	124.4	271.0	207.7	347.1	126.2

As already outlined in the Introduction, a key motivation for investigating ternary cadmium chalcogenides lies in the possibility of tailoring their band gaps by varying the composition [9,10]. Generally, the band gap width of bulk CsS is reported to be 2.42 eV, while that of CdSe is 1.74 eV, although variations exist in the literature due to size effects and sample morphology. As expected, there are variations in values reported throughout the literature, with the band gap increasing with decreasing nanoparticles size due to the quantum confinement effect [46]. On the other hand, CdS thin films have been reported with slightly reduced band gap values in the 2.27 – 2.33 eV range [47].

In ternary systems, the band gap typically falls between those of the two binary end members, but the relationship is often nonlinear due to the so-called *bowing effect* [48]. For the CdS_xSe_{1-x} system, the deviation from linearity is relatively small, since CdS and CdSe are miscible with almost zero enthalpy change due to small lattice mismatch [49]. By contrast, the CdS_xTe_{1-x} system exhibits a more complex dependence, with some of the ternary compositions reported to display either broader or narrower band gaps than any of the binaries [50,51]. Similar behavior was reported for the $CdSe_xTe_{1-x}$ system, which has gained considerable attention in photovoltaic research, as partial incorporation of CdSe into CdTe thin film solar cells has been shown to improve cell performance [52,53]. At first glance, using a 1.74 eV band gap CdSe to increase the optical absorption of CdTe (E_g = 1.45 eV) seems counterintuitive, however alloying of CdSe into CdTe can effectively reduce the band gap below the values of either of the binary compounds due to the large bowing effect [54].

In the present work, the optical band gap energies of ternary cadmium chalcogenides were determined from UV–Vis absorption spectra using *Tauc* plots, according to the relation:

$$(\alpha h\nu)^n = A(h\nu - E_g)$$

Here, α is the absorption coefficient (cm^{-1}), $h\nu$ the photon energy (eV), A is a constant, and $n = 2$ for a direct transition. By plotting $(\alpha h\nu)^2$ vs. $(h\nu)$ and extrapolating the linear portion of the curve to the x-axis, the band gap value E_g (eV) can be obtained as the intercept [40,46,47,49].

 doi:10.20944/preprints202510.0291.v1

The optical band gap energies, calculated for $CdS_{0.5}Se_{0.5}$, $CdS_{0.5}Te_{0.5}$, and $CdSe_{0.5}Te_{0.5}$, were 2.01 eV, 1.72 eV, and 1.53 eV, respectively, as presented in Figure 12. The value obtained for $CdS_{0.5}Se_{0.5}$ fits perfectly between the values of the binaries, while being slightly higher when compared to the values of 1.8 – 1.95 eV reported in literature [48,49]. In contrast, the measured band gap value of $CdS_{0.5}Te_{0.5}$ is slightly lower than the values of 1.88–1.94 eV previously reported [50,55], though still in reasonable agreement. Finally, the result measured for $CdSe_{0.5}Te_{0.5}$ (= 1.53 eV) matches perfectly with ≈ 1.55 eV, reported in [56]. These findings support the expected tunability of band gaps in ternary cadmium chalcogenides and further confirm the successful synthesis of the targeted compositions.

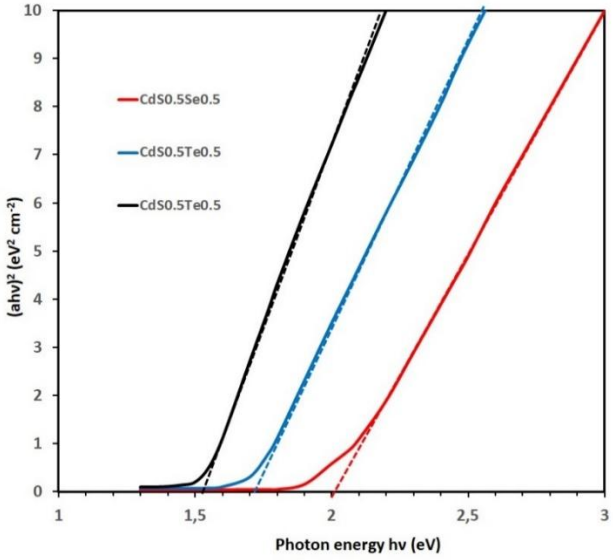

Figure 12. Tauc plots used for the determination of band gaps for $CdS_{0.5}Se_{0.5}$, $CdS_{0.5}Te_{0.5}$, and $CdSe_{0.5}Te_{0.5}$.

4. Conclusions

Binary and ternary cadmium chalcogenides were successfully synthesized from elemental precursors using a mechanochemical approach. Powder XRD and DSC analyses confirmed the complete formation of CdS, CdSe, and CdTe within 15 min of milling, with phase purity for CdS and CdSe achievable under an inert atmosphere to prevent oxidation. Ternary alloys, namely, $CdS_{0.5}Se_{0.5}$, $CdS_{0.5}Te_{0.5}$, and $CdSe_{0.5}Te_{0.5}$, were successfully synthesized and their compositions confirmed by pXRD and AAS measurements, while their diffraction patterns indicate the formation of homogeneous solid solutions, free from detectable oxide impurities.

TEM imaging revealed that the products consist of irregular aggregates of several hundred nanometers, composed of smaller spherical primary nanoparticles in the 10–20 nm range, consistent with crystallite sizes estimated from XRD. DLS measurements in aqueous suspensions indicated larger hydrodynamic diameters, as expected due to particle solvation and aggregation. UV–Vis spectroscopy demonstrated tunable optical band gaps in the ternary systems, with measured values in good agreement with literature reports and consistent with expected bowing effects.

Overall, mechanochemical synthesis proves to be a simple, rapid, and environmentally friendly method for preparing binary and ternary cadmium chalcogenides, avoiding solvents, toxic precursors, and high-temperature treatments. The tendency of the products to form aggregates may be mitigated in future work through the use of surfactants or optimized milling protocols, enabling improved control over particle size and dispersion for potential applications in optoelectronic devices.

Author Contributions: Conceptualization, M.K. and J.S.; Methodology, M.K., S.G. and J.S.; Investigation, M.K.; N.Z.; J.K.; and S.G.; Supervision, M.K. and J.S.; Writing-original draft preparation, M.K.; Writing-review and editing, M.K. and J.S. All authors have read and agreed to the published version of the manuscript.

 doi:10.20944/preprints202510.0291.v1

Funding: The authors acknowledge the financial support from the grant number P2-0006 of the Slovenian Research Agency (ARIS).

Data Availability Statement: The original contributions presented in the study are included in the article, further inquiries can be directed to the corresponding author.

Acknowledgments: The first author would like to thank Janja Kristl for performing UV-Vis and AAS analysis, and Sabina Vohl for DLS measurements and evaluation as well as for coordinating the work of N.Z. and J.K. in the laboratory.

Conflicts of Interest: The authors declare no conflicts of interest.

Abbreviations

The following abbreviations are used in this manuscript:

pXRD	Powder X-ray Diffraction
DSC	Differential Scanning Calorimetry
TEM	Transmission Electron Microscopy
EDX	Energy-Dispersive X-ray Spectroscopy
DLS	Dynamic Light Scattering
AAS	Atomic Absorption Spectroscopy

References

1. Maity, R.; Kundoo, S.; Chattopadhyay, K.K. Synthesis and Optical Characterization of CdS Nanowires by Chemical Route. *Mater. Manuf. Process.* **2006**, *21*, 644–647. https://doi.org/10.1080/10426910600611458
2. Isa, A.T; Hafeez, H.Y.; Mohammed, J.; Kafadi, A.D.G.; Ndikilar, C.E.; Suleiman, A.B. A review on the progress and prospect of CdS-based photocatalysts for hydrogen generation via photocatalytic water splitting. *J. Alloy. Comp. Comm*. **2024**, *4*, 100043. https://doi.org/10.1016/j.jacomc.2024.100043
3. Suhaimi, N.H.S; Syed, J.A.S.; Azhar, R.; Adzis, N.S.; Halim, O.M.A.; Chang, Y.H.R.; Taylor, S.H.; Bailey, L.A.; Ab Rahim, M.H.; Ramli, M.Z.; Nawawi, W.I.; Ishak, M.A.M. Perspective on CdS-based S-scheme photocatalysts for efficient photocatalytic applications: Characterisation techniques and optimal semiconductor coupling. *Int. J. Hydrogen Energy* **2025**, *165*, 150929. https://doi.org/10.1016/j.ijhydene.2025.150929
4. Mamiyev, Z.; Balayeva, N.O. Metal Sulfide Photocatalysts for Hydrogen Generation: A Review of Recent Advances. *Catalysts* **2022**, *12*, 1316. https://doi.org/10.3390/catal12111316
5. Li, J.; Zheng, H.; Zheng, Z.; Rong, H.; Zeng, Z.; Zeng, H. Synthesis of CdSe and CdSe/ZnS Quantum Dots with Tunable Crystal Structure and Photoluminescent Properties. *Nanomaterials* **2022**, *12*, 2969. https://doi.org/10.3390/nano12172969
6. Khan, I.; Ali, A.; Ul Haq, I.; Abdul Aziz, S.; Ali, Z.; Ahmad, I. The effect of potassium insertion on optoelectronic properties of cadmium chalcogenides, *Mater. Sci. Semicond. Process*. **2021**, *122*, 105466. https://doi.org/10.1016/j.mssp.2020.105466.
7. Rojas, J.A.; Oliva, A.I. A Double Energy Transition of Nanocrystalline $Cd_xZn_{1-x}S$ Films Deposited by Chemical Bath. *Mater. Manuf. Process.* **2015**, *30*, 785–792. https://doi.org/10.1080/10426914.2014.994776
8. Aldakov, D.; Lefrançois, A.; Reiss, P. Ternary and quaternary metal chalcogenide nanocrystals: synthesis, properties and applications. *J. Mater. Chem. C 2013*, *1*, 3756-3776. https://doi.org/10.1039/C3TC30273C
9. Ebrahim, F.; Al-Hartomy, O.; Wageh, S. Cadmium-Based Quantum Dots Alloyed Structures: Synthesis, Properties, and Applications. *Materials* **2023**, *16*, 5877. https://doi.org/10.3390/ma16175877
10. Moger, S.N.; Mahesha, M. G. Colour tunable co-evaporated CdS_xSe_{1-x} ($0 \le x \le 1$) ternary chalcogenide thin films for photodetector applications. *Mater. Sci. Semicond. Process*. **2020**, *120*, 105288. https://doi.org/10.1016/j.mssp.2020.105288
11. Diker, H.; Unluturk, S.S.; Ozcelik, S.; Varlikli, C. Improving the Stability of Ink-Jet Printed Red QLEDs By Optimizing The Device Fabrication Process. *Nanofabrication* **2024**, *9*. https://doi.org/10.37819/nanofab.9.1822

 doi:10.20944/preprints202510.0291.v1

12. Jiang, Y.; Wang, Z.; Wang, S.; Zhang, C.; Luan, C.; Chen, X.; Yu, K. Development of aqueous-phase CdSeS magic-size clusters at room temperature and quantum dots at elevated temperatures. *Nano Res.* **2024**, *17*, 10529–10535. https://doi.org/10.1007/s12274-024-6884-y
13. Abu-Farsakh, H.; Gul, B.; Khan, M.S. Investigating the Optoelectronic and Thermoelectric Properties of CdTe Systems in Different Phases: A First-Principles Study. *ACS Omega* **2023**, *8*, 14742-14751. https://doi.org/10.1021/acsomega.3c00757
14. Romeo, A.; Artegiani, E. CdTe-Based Thin Film Solar Cells: Past, Present and Future. *Energies* **2021**, *14*, 1684. https://doi.org/10.3390/en14061684
15. Bosio, A.; Rosa, G.; Romeo, N. Past, present and future of the thin film CdTe/CdS solar cells. *Sol. Energy* **2018**, *175*, 31-43. https://doi.org/10.1016/j.solener.2018.01.018.
16. Scarpulla, M.A.; McCandless, B.; Phillips, A.B.; Yan, Y.; Heben, M.J.; Wolden, C.; Xiong, G.; Metzger, W.K.; Mao, D.; Krasikov, D.; Sankin, I.; Grover, S.; Munshi, A.; Sampath, W.; Sites, J.R.; Bothwell, A.; Albin, D.; Reese, M.O.; Romeo, A.; Nardone, M.; Klie, R.; J. Walls, J.M.; Fiducia, T.; Abbas, A.; Hayes, S.M. CdTe-based thin film photovoltaics: Recent advances, current challenges and future prospects. *Sol. Energy Mater. Sol. Cells* **2023**, *255*, 112289. https://doi.org/10.1016/j.solmat.2023.112289.
17. Sivasankar, S.M.; Amorim, C.d.O.; Cunha, A.F.d. Progress in Thin-Film Photovoltaics: A Review of Key Strategies to Enhance the Efficiency of CIGS, CdTe, and CZTSSe Solar Cells. *J. Compos. Sci.* **2025**, *9*, 143. https://doi.org/10.3390/jcs9030143
18. Jamaatisomarin, F.; Chen, R.; Hosseini-Zavareh, S.; Lei, S. Laser Scribing of Photovoltaic Solar Thin Films: A Review. *J. Manuf. Mater. Process.* **2023**, *7*, 94. https://doi.org/10.3390/jmmp7030094
19. Pinto, A.H.; Cho, D.Y.; Oliynyk, A.O.; Silverman, J.R. Green Chemistry Applied to Transition Metal Chalcogenides through Synthesis, Design of Experiments, Life Cycle Assessment, and Machine Learning. Green Chemistry - New Perspectives. IntechOpen; **2022**. Available from: http://dx.doi.org/10.5772/intechopen.104432
20. Ghasempour, A.; Dehghan, H.; Ataee, M.; Chen, B.; Zhao, Z.; Sedighi, M.; Guo, X.; Shahbazi, M.-A. Cadmium Sulfide Nanoparticles: Preparation, Characterization, and Biomedical Applications. *Molecules* **2023**, *28*, 3857. https://doi.org/10.3390/molecules28093857
21. Buckingham, M.A.; Norton, K.; McNaughter, P.D.; Whitehead, G.; Vitorica-Yrezabal, I.; Alam, F.; Laws, K.; Lewis, D.J. Investigating the Effect of Steric Hindrance within CdS Single-Source Precursors on the Material Properties of AACVD and Spin-Coat-Deposited CdS Thin Films. *Inorg. Chem.* **2022**, *61*, 8206–8216. https://doi.org/10.1021/acs.inorgchem.2c00616
22. Karmakar, G.; Tyagi, A.; Shah, A.Y. A comprehensive review on single source molecular precursors for nanometric group IV metal chalcogenides: Technologically important class of compound semiconductors. *Coord. Chem. Rev*. 2024, *504*, 215665. https://doi.org/10.1016/j.ccr.2024.215665
23. Dojer, B.; Pevec, A.; Breznik, K.; Jagličić, Z.; Gyergyek, S.; Kristl, M. Structural and thermal properties of new copper and nickel single-source precursors. *J. Mol. Struct*. **2019**, *1194*, 171-177. https://doi.org/10.1016/j.molstruc.2019.05.047
24. Kristl, M.; Ban, I.; Danč, A.; Danč, V.; Drofenik, M. A sonochemical method for the preparation of cadmium sulfide and cadmium selenide nanoparticles in aqueous solutions. *Ultrason. Sonochem*. **2010**, *17*, 916-922. https://doi.org/10.1016/j.ultsonch.2009.12.013
25. Ban, I.; Kristl, M.; Danč, V.; Danč, A.; Drofenik, M. Preparation of cadmium telluride nanoparticles from aqueous solutions by sonochemical method. *Mater. Lett*. **2012**, *67*, 56-59. https://doi.org/10.1016/j.matlet.2011.09.001
26. Palanisamy, B.; Paul, B.; Chang, C.-H. The synthesis of cadmium sulfide nanoplatelets using a novel continuous flow sonochemical reactor. *Ultrason. Sonochem.* **2015**, *26*, 452-460. https://doi.org/10.1016/j.ultsonch.2015.01.004
27. Denac, B.; Kristl, M.; Gyergyek, S.; Drofenik, M. Preparation and characterization of ternary cadmium chalcogenides. *Chalcogenide Lett*. **2013**, *10*, 87-98.
28. Shalabayev, Z.; Baláž, M.; Khan, N.; Nurlan, Y.; Augustyniak, A.; Daneu, N.; Tatykayev, B.; Dutková, E.; Burashev, G.; Casas-Luna, M.; et al. Sustainable Synthesis of Cadmium Sulfide, with Applicability in

 doi:10.20944/preprints202510.0291.v1

Photocatalysis, Hydrogen Production, and as an Antibacterial Agent, Using Two Mechanochemical Protocols. *Nanomaterials* **2022**, *12*, 1250. https://doi.org/10.3390/nano12081250

29. Gancheva, M.; Iordanova, R.; Ivanov, P.; Yordanova, A. Effect of Ball Milling Speeds on the Phase Formation and Optical Properties of α-$ZnMoO_4$ and ß-$ZnMoO_4$ Nanoparticles. *J. Manuf. Mater. Process.* **2025**, *9*, 118. https://doi.org/10.3390/jmmp9040118
30. Pagola, S. Outstanding Advantages, Current Drawbacks, and Significant Recent Developments in Mechanochemistry: A Perspective View. *Crystals* **2023**, *13*, 124. https://doi.org/10.3390/cryst13010124
31. Fantozzi, N.; Volle, J.-N.; Porcheddu, A.; Virieux, D.; Garcia, F.; Colacino, E. Green metrics in mechanochemistry. *Chem. Soc. Rev.* **2023**, *52*, 6680-6714. https://doi.org/10.1039/D2CS00997H
32. Mukherjee, N. Mechanochemistry: A Resurgent Force in Chemical Synthesis. *Synlett* **2024**, *35*, 2331-2345. https://doi.org/10.1055/a-2422-0992
33. Martinez, V., Stolar, T., Karadeniz, B., Brekalo, I., Užarević, K. Advancing mechanochemical synthesis by combining milling with different energy sources. *Nat. Rev. Chem.* **2023**, 7, 51–65. https://doi.org/10.1038/s41570-022-00442-1
34. Dubadi, R.; Huang, S.D.; Jaroniec, M. Mechanochemical Synthesis of Nanoparticles for Potential Antimicrobial Applications. *Materials* **2023**, *16*, 1460. https://doi.org/10.3390/ma16041460
35. Tan, G.L.; Hömmerich, U.; Temple, D.; Wu, N.Q.; Zheng, J.G.; Loutts, G. Synthesis and optical characterization of CdTe nanocrystals prepared by ball milling process. *Scr. Mater*. **2003**, *48*,1469-1474. https://doi.org/10.1016/S1359-6462(03)00079-4
36. Campos, C.E.M. Solid State Synthesis and Characterization of NiTe Nanocrystals. *J. Nano Res.* **2014**, *29*, 35-39. https://doi.org/10.4028/www.scientific.net/JNanoR.29.35
37. Baláž, M.; Džunda, R.; Bureš, R.; Sopčák, T.; Csanádi, T. Mechanically induced self-propagating reactions (MSRs) to instantly prepare binary metal chalcogenides: assessing the influence of particle size, bulk modulus, reagents melting temperature difference and thermodynamic constants on the ignition time. *RSC Mechanochem.* **2024**,*1*, 94-105. https://doi.org/10.1039/D3MR00001J
38. Kristl, M.; Ban, I.; Gyergyek, S. Preparation of Nanosized Copper and Cadmium Chalcogenides by Mechanochemical Synthesis. *Mater. Manuf. Process.* **2013**, *28*, 1009–1013. https://doi.org/10.1080/10426914.2013.811736
39. Kristl, M.; Gyergyek, S.; Srt, N.; Ban, I. Mechanochemical Route for the Preparation of Nanosized Aluminum and Gallium Sulfide and Selenide. *Mater. Manuf. Process.* **2016**, *31*, 1608–1612. https://doi.org/10.1080/10426914.2015.1103860
40. Kristl, M.; Gyergyek, S.; Škapin, S.D.; Kristl, J. Solvent-Free Mechanochemical Synthesis and Characterization of Nickel Tellurides with Various Stoichiometries: NiTe, $NiTe_2$ and Ni_2Te_3. *Nanomaterials* **2021**, *11*, 1959. https://doi.org/10.3390/nano11081959
41. Salvador, A.; Pascual-Martí, M.C.; Aragó, E.; Chisvert, A.; March, J.G. Determination of selenium, zinc and cadmium in antidandruff shampoos by atomic spectrometry after microwave assisted sample digestion. *Talanta* **2000**, *51*, 1171-1177. https://doi.org/10.1016/S0039-9140(00)00290-3
42. Souaya, E.R.; Elkholy, S.A.; Abd El-Rahman, A.M.M.; El-Shafie, M.; Ibrahim, I.M.; Abo-Shanab, Z.L. Partial substitution of asphalt pavement with modified sulfur. *Egypt. J. Pet.* **2015**, *24*, 483-491. https://doi.org/10.1016/j.ejpe.2015.06.003.
43. Triboulet, R. Fundamentals of the CdTe synthesis. *J. Alloys Compd.* **2004**, *371*, 67-71. https://doi.org/10.1016/j.jallcom.2003.06.006.
44. Ban, I.; Markuš, S.; Gyergyek, S.; Drofenik, M.; Korenak, J.; Helix-Nielsen, C.; Petrinić, I. Synthesis of Poly-Sodium-Acrylate (PSA)-Coated Magnetic Nanoparticles for Use in Forward Osmosis Draw Solutions. *Nanomaterials* **2019**, *9*, 1238. https://doi.org/10.3390/nano9091238
45. Larichev, Y.V. Application of DLS for metal nanoparticle size determination in supported catalysts. *Chem. Pap.* **2021**, *75*, 2059–2066. https://doi.org/10.1007/s11696-020-01454-1
46. Praus, P.; Kozák, O.; Kočí, K.; Panáček, A.; Dvorský, R. CdS nanoparticles deposited on montmorillonite: Preparation, characterization and application for photoreduction of carbon dioxide. *J. Colloid Interface Sci.* **2011**, *360*, Issue 2, 574-579. https://doi.org/10.1016/j.jcis.2011.05.004

 doi:10.20944/preprints202510.0291.v1

47. Sinha, T.; Verma, L.; Khare, A. Variations in photovoltaic parameters of CdTe/CdS thin film solar cells by changing the substrate for the deposition of CdS window layer. *Appl. Phys. A* **2020,** *126*, 867. https://doi.org/10.1007/s00339-020-04058-4
48. Shoaib, M., Wang, X., Zhang, X.; Zhang, Q.; Pan A. Controllable Vapor Growth of Large-Area Aligned CdS_xSe_{1-x} Nanowires for Visible Range Integratable Photodetectors. *Nano-Micro Lett.* **2018**, *10*, 58. https://doi.org/10.1007/s40820-018-0211-7
49. Tyagi, J.; Gupta, H.; Purohit, L.P. Ternary alloyed $CdS_{1-x}Se_x$ quantum dots on TiO_2/ZnS electrodes for quantum dots-sensitized solar cells. *J. Alloys Compd*. **2021**, *880*,160480. https://doi.org/10.1016/j.jallcom.2021.160480.
50. Mezrag, F.; Bouarissa, N.; El-Houda Fares, N. The band gap bowing of CdS_xTe_{1-x} alloys beyond the virtual crystal approximation. *Emerg. Mater. Res.* **2020**, *9*, 1056–1059. https://doi.org/10.1680/jemmr.19.00187
51. Lane, D.W. A review of the optical band gap of thin film CdS_xTe_{1-x}. *Sol. Energy Mater. Sol. Cells* **2006**, *90*, 1169-1175. https://doi.org/10.1016/j.solmat.2005.07.003
52. Baines, T.; Zoppi, G.; Bowen, L.; Shalvey, T.P.; Mariotti, S.; Durose, K.; Major, J.D. Incorporation of CdSe layers into CdTe thin film solar cells. *Sol. Energy Mater. Sol. Cells* **2018**, *180*,196-204. https://doi.org/10.1016/j.solmat.2018.03.010
53. Song, X.; Ma, Z.; Li, L.; Tian, T.; Yan, Y.; Su, J.; Deng, J.; Xia, C. Aqueous synthesis of alloyed $CdSe_xTe_{1-x}$ colloidal quantum dots and their In-situ assembly within mesoporous TiO_2 for solar cells. *Sol. Energy* **2020**, *196*, 513-520. https://doi.org/10.1016/j.solener.2019.12.049
54. Yang, X.; Wei, S.-H. First-principles study of the band gap tuning and doping control in $CdSe_xTe_{1-x}$ alloy for high efficiency solar cell. *Chinese Phys. B* **2019**, *28*, 086106. https://doi.org/10.1088/1674-1056/28/8/086106
55. Hoa, N.M., Thi, L.A., Hung, L.X., Toan, L.D. Tunable excitonic dynamics and photoluminescence modulation in graded CdSe/CdSeS quantum dots for optoelectronic applications. *J. Mater. Sci.: Mater. Electron.* **2025**, *36*, 1539. https://doi.org/10.1007/s10854-025-15610-4
56. Kashuba, A.I.; Andriyevsky, B. Growth and crystal structure of $CdTe_{1-x}Se_x$ ($x \geq 0.75$) thin films prepared by the method of high-frequency magnetron sputtering. *Low Temp. Phys.* **2024**, *50*, 29–33. https://doi.org/10.1063/10.0023888